BIOCHEMISTRY
including biophysical chemistry & molecular biology

Article

pubs.acs.org/biochemistry

Probing the Effects of DNA–Protein Interactions on DNA Hole Transport: The N-Terminal Histone Tails Modulate the Distribution of Oxidative Damage and Chemical Lesions in the Nucleosome Core Particle

William B. Davis,* Chad C. Bjorklund,† and Marshall Deline

School of Molecular Biosciences, Biotechnology/Life Sciences 135, Washington State University, Pullman, Washington 99164-7520, United States

Supporting Information

ABSTRACT: The ability of DNA to transport positive charges, or holes, over long distances is well-established, but the mechanistic details of how this process is influenced by packaging into DNA–protein complexes have not been fully delineated. In eukaryotes, genomic DNA is packaged into chromatin through its association with the core histone octamer to form the nucleosome core particle (NCP), a complex whose structure can be modulated through changes in the local environment and the histone proteins. Because (i) varying the salt concentration and removing the histone tails influence the structure of the NCP in known ways and (ii) previous studies have shown that DNA hole transport (HT) occurs in the nucleosome, we have used our previously described 601 sequence NCPs to test the hypothesis that DNA HT dynamics can be modulated by structural changes in a DNA–protein complex. We show that at low salt concentrations there is a sharp increase in long-range DNA HT efficiency in the NCP as compared to naked DNA. This enhancement of HT can be negated by either removal of the histone tails at low salt concentrations or disruption of the interaction of the packaged DNA and the histone tails by increasing the buffer's ionic strength. Association of the histone tails with 601 DNA at low salt concentrations shifts the guanine damage spectrum to favor lesions like 8-oxoguanine in the NCP, most likely through modulation of the rate of the reaction of the guanine radical cation with oxygen. These experimental results indicate that for most genomic DNA, the influence of DNA–protein interactions on DNA HT will depend strongly on the level of protection of the DNA nucleobases from oxygen. Further, these results suggest that the oxidative damage arising from DNA HT may vary in different genomic regions depending on the presence of either euchromatin or heterochromatin.

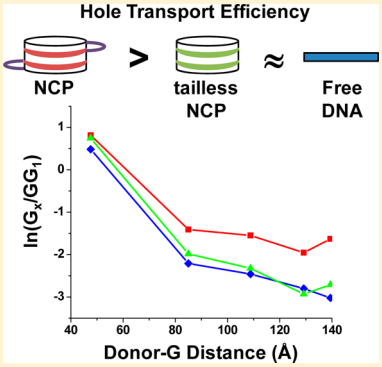

The movement of excess charge, both electrons and holes, through the DNA base stack is a well-established phenomenon from numerous experimental and theoretical studies performed over the past several decades.[1−4] In vitro and in silico studies of DNA hole transport (HT) have led to several competing frameworks for understanding how DNA sequence, structure, and local environment impact the dynamics of this process.[5−10] All current models for DNA HT are built on the following generalities. (1) Because guanine has the lowest oxidation potential in DNA,[11] it is the preferred site for hole localization in DNA (the guanine radical cation, $G^{\bullet+}$, is its one-electron oxidation product), and (2) the local sequence around a guanine will influence its oxidation propensity, with 5′-GG and 5′-GGG sites serving as deeper hole traps than single guanines.[12−14] The steady state distribution of oxidative lesions that arise from DNA HT is determined by the relative kinetics of two competing processes at each guanine residue. First, there are the rates of hole hopping (k_{hop}) between the guanine residues. The time scales of hopping between guanines are expected to be on the nanosecond to microsecond time scale, and the microscopic rates will depend on the intervening DNA sequence, local DNA structure, and number of consecutive guanine residues at each oxidation site.[15,16] The second process that controls DNA HT is the rate of hole trapping by chemical reaction of $G^{\bullet+}$ with either water (k_{H_2O}) or oxygen (k_{O_2}), reactions expected to occur on the microsecond time scale.[17,18]

The vast majority of the studies on DNA HT have utilized DNA duplexes either free in buffered aqueous media or anchored to solid state electrochemical devices. The results of these experiments have naturally led to questions about the feasibility of this process in biological contexts. Support for the existence of DNA HT in cellulo was recently provided by experiments showing that treatment of cells with a photo-oxidant known to intercalate and initiate DNA HT leads to nuclear[19] and mitochondrial[20,21] DNA damage distributions resembling those that arise from long-range hole transport. Because DNA is not found in a naked state in the cell, it is

Received: November 21, 2011
Revised: March 5, 2012
Published: March 12, 2012

necessary to perform experimental and theoretical analyses of DNA HT in well-characterized DNA–protein complexes to understand the biological impact of this process. Prior studies along these lines have studied DNA HT in complexes involving transcription factors,[22,23] restriction endonucleases,[24,25] DNA repair factors,[26] and structural proteins.[27−30] In cellulo, DNA–protein interactions are dynamic and vary throughout the cell cycle to affect DNA-based biochemical processes like replication, DNA repair, and transcriptional regulation.

The plasticity of DNA–protein binding is highlighted exquisitely by the nucleosome core particle (NCP), the DNA–histone complex that serves as the fundamental building block of chromatin packaging in the eukaryotic nucleus.[31] Complex, dynamic combinations of histone sequence variants, post-translational modifications of the histone tails and folded core domains, and bound non-histone regulatory proteins give rise to controlled transitions between two extremes of genomic structure: (1) tightly packaged regions, or heterochromatin, at, e.g., telomeres and centromeres, and (2) relatively open areas (euchromatin) at sites of active transcription.[32] Because the formation of the NCP is a highly reversible reaction, due to the electrostatic interactions that stabilize this complex, the fundamental thermodynamic and kinetic properties of the NCP have been delineated using controlled changes in pH or bulk salt concentration. Additional experiments with mononucleosomes and oligonucleosome arrays have shown that the basic histone N-terminal and C-terminal tails play an important role in stabilizing chromatin structure and that either their removal or their chemical modification will lead to dramatic changes in DNA–protein interactions.[33]

In this study, we have chosen to use the NCP, a well-characterized biochemical system, to study how DNA packaging affects the dynamics of long-range DNA HT. In particular, we tested the hypothesis that the sensitivity of DNA HT to environmental changes can be used to map structural changes in DNA–protein complexes. Using our previously described AQ-601 DNA HT construct,[29,34] we tested our hypothesis by correlating (i) the effects of varying bulk salt concentration and histone tail removal on long-range DNA HT efficiency and final oxidative product distribution with (ii) the known changes in NCP structure induced by these treatments.

EXPERIMENTAL PROCEDURES

Preparation of Naked DNA Samples. An anthraquinone (AQ)-modified, 162 bp duplex containing the 601 strong nucleosome positioning sequence (AQ-601) was prepared by polymerase chain reaction and radiolabled at the free 5′-end using protocols described previously.[29] Naked AQ-601 samples were first prepared in 10 mM phosphate (pH 7.0), 1000 mM NaCl buffer, and 50 μL aliquots were dialyzed for 1 h at 4 °C against 10 mM phosphate buffer (pH 7.0) with a NaCl concentration of either 10, 200, 400, 600, 800, or 1000 mM.[34]

Preparation of AQ-601 Nucleosome Samples (rAQ-601). The preparation of chicken erythrocyte nucleosome core particles reconstituted with 5′-^{32}P-labeled AQ-601 was performed as previously described with slight modifications.[28,29] First, AQ-601 and a large molecular excess of purified nucleosome core particles (obtained using chicken red blood cells, Lampire Biological Products) were mixed in 1× TE, 1000 mM NaCl buffer on ice and then dialyzed against 10 mM phosphate (pH 7.0), 1000 mM NaCl buffer for 1 h at 4 °C. To generate rAQ-601 samples at lower salt concentrations, we performed a series of dialysis steps against buffers of decreasing salt concentration at 4 °C. For example, to generate samples at 200 mM NaCl, rAQ-601 was sequentially dialyzed against 800, 400, and 200 mM NaCl buffers. An electrophoretic mobility shift assay (EMSA) on 6% native polyacrylamide gel electrophoresis (PAGE) gels (Figure S1 of the Supporting Information) was used to determine the efficiency of NCP reconstitution at all salt concentrations.

Preparation of Tailless rAQ-601 Samples (trAQ-601). Tailless chicken erythrocyte nucleosomes were prepared by limited trypsin digestion.[28] The tailless histones were reconstituted with AQ-601 as described in the preceding section and dialyzed stepwise into a final buffer of 10 mM phosphate (pH 7.0) and 10 mM NaCl, and the reconstitution efficiency was checked using EMSA gels (Figure S2 of the Supporting Information).

Photochemical DNA HT Assays. DNA HT was initiated in all samples by placing samples in nonsilanized 1.5 mL tubes (Fisher) and irradiating them in a UV-A photoreactor with a rotating sample carousel (Luzchem).[28,29] Following irradiation, all samples were incubated at 37 °C with proteinase K to digest protein and extracted with a phenol/chloroform/isoamyl alcohol mixture. After ethanol precipitation using glycogen as a carrier, the DNA was resuspended in 50 μL of freshly distilled piperidine and incubated at 90 °C for 30 min. Samples were next evaporated and washed two times with water and then resuspended in formamide loading buffer. Following separation of the DNA fragments on 7 M urea–6% PAGE DNA sequencing gels (Figure S3 of the Supporting Information), the gels were placed in a storage phosphor screen (Bio-Rad) and scanned using a Storm Phosphorimager and Imagequant (GE Healthcare). The amount of radioactivity in each band (r_x), including the parent, was determined by subtracting the integrated volume of ellipses drawn around identical locations in lanes containing irradiated and nonirradiated, but otherwise identically treated, samples. For each GG or GGG site, the radioactivities of the cleavage products at all of the individual guanine residues were summed together to produce a single value. The percent damage at each guanine site was calculated using the equation: percent damage at site $G_x = r_x/\sum r_i$ (i spans all guanine damage bands). An alternative way to represent our data was to calculate G_x/GG_1 ratios using $G_x/GG_1 = r_x/r_{GG_1}$. All reported means and standard errors of the mean (SEM) were calculated from three technical replicates.

To quantify the relative ratios of guanine lesions arising from O_2-dependent and H_2O-dependent trapping pathways, we treated DNA samples using either piperidine or formamidopyrimidine-DNA glycosylase (FPG) (Trevigen).[35] After UV-A irradiation, proteinase K treatment, phenol/chloroform extraction, and ethanol precipitation, DNA was resuspended in water and the sample split in half. After the water had been removed from the first aliquot of DNA, the DNA was resuspended in piperidine, dried, washed twice with water, and finally resuspended in formamide gel loading buffer. To the second half of the sample we added a $^1/_{10}$ volume of 10× FPG buffer and then 10 units of FPG (New England Biolabs). The samples were incubated at 37 °C for 1 h, followed by phenol extraction, ethanol precipitation, and resuspension in formamide loading buffer. Piperidine- and FPG-treated samples were run side by side on 7 M urea–6% PAGE DNA sequencing gels (Figure S4 of the Supporting Information), and as described previously, the amount of radioactivity in each band was determined using autoradiography and the percent damage at each guanine site in

the FPG- and piperidine-treated samples calculated. To calculate the yield of FPG lesions at site G_x (Y_{FPG}), we divided r_x by the sum of the radioactivity of all the bands, including the parent, in that lane. A similar procedure was used to calculate the yield of piperidine lesions at each site G_x (Y_{pip}). These Y_{FPG} and Y_{pip} values were then used to calculate the Y_{pip}/Y_{FPG} ratio at each guanine site in the naked, nucleosomal, and tailless nucleosome AQ-601 samples. All experimental data are reported as the means and SEM calculated from three technical replicates.

RESULTS

Generation and Structural Characterization of AQ-601 NCPs. We previously published[29] the experimental procedures used to generate reconstituted AQ-601 (Figure 1A) NCPs (rAQ-601) in 10 mM phosphate (pH 7.0), 10 mM NaCl buffer. We used the following rationales for using the AQ-601 construct to study DNA HT in the nucleosome: (1) It has an end-capping AQ photooxidant[36] at one 5′ terminus to initiate DNA HT at a known location. (2) The 601 sequence forms NCPs of high thermodynamic stability with only one rotational and one translational setting.[37] (3) A 15 bp DNA linker region between AQ and the start of the 601 sequence places the photooxidant outside of the DNA−histone contact regions to minimize spurious AQ−nucleosome interactions. (4) It has multiple guanine oxidation sites [labeled GG_1−G_7 (Figure 1A)]. (5) The 5′-^{32}P label on the AQ counterstrand allows the use of sensitive autoradiography techniques to quantify the relative levels of guanine damage caused by DNA HT (Figure 1B). To study DNA HT in rAQ-601 and naked AQ-601 as a function of salt, we modified our previously published[29] stepwise salt dialysis protocol to generate samples in 10 mM phosphate buffer (pH 7.0) with 10, 200, 400, 600, 800, or 1000 mM salt. From native PAGE gels (Figure S1 of the Supporting Information), AQ-601 is associated with histone proteins at all salt concentrations between 10 and 1000 mM. From autoradiography, the efficiency of rAQ-601 production was >90% at all salt concentrations except 1000 mM, where the efficiency decreased to ∼80%. The decrease in rAQ-601 production at the highest salt concentration is attributed to electrostatic destabilization of the histone octamer because of the loss of histone H2A−H2B dimers between 800 and 1000 mM NaCl.[38] Also, the EMSA gels show neither a significant accumulation of material near the wells nor DNA-containing complexes that migrate slower than the nucleosome. This result provides evidence that our rAQ-601 samples do not aggregate, and it is consistent with the previous observation that mononucleosomes reconstituted with DNA fragments up to 165 bp in length do not form multinucleosome aggregates at any salt concentration.[39] Therefore, changes in DNA HT in rAQ-601 versus naked AQ-601 will be assigned to intra-nucleosome and not internucleosome effects.

Combining the recently published crystal structures of 601 NCPs[40,41] and our hydroxyl radical and exonuclease III footprinting data for rAQ-601,[29] we generated a refined structural model for rAQ-601 using VMD (Figure 1C).[42] In this model, the AQ photooxidant and the adjacent 15 bp of DNA (including sites GG_1 and GGG_2) are not associated with the folded histone domains and are therefore not shown in Figure 1C. This region will henceforth be termed the DNA "linker" because it mimics genomic DNA found between nucleosomes. Using the crystal structure as a model, sites GGG_3−G_7 are in the first three turns of DNA associated with

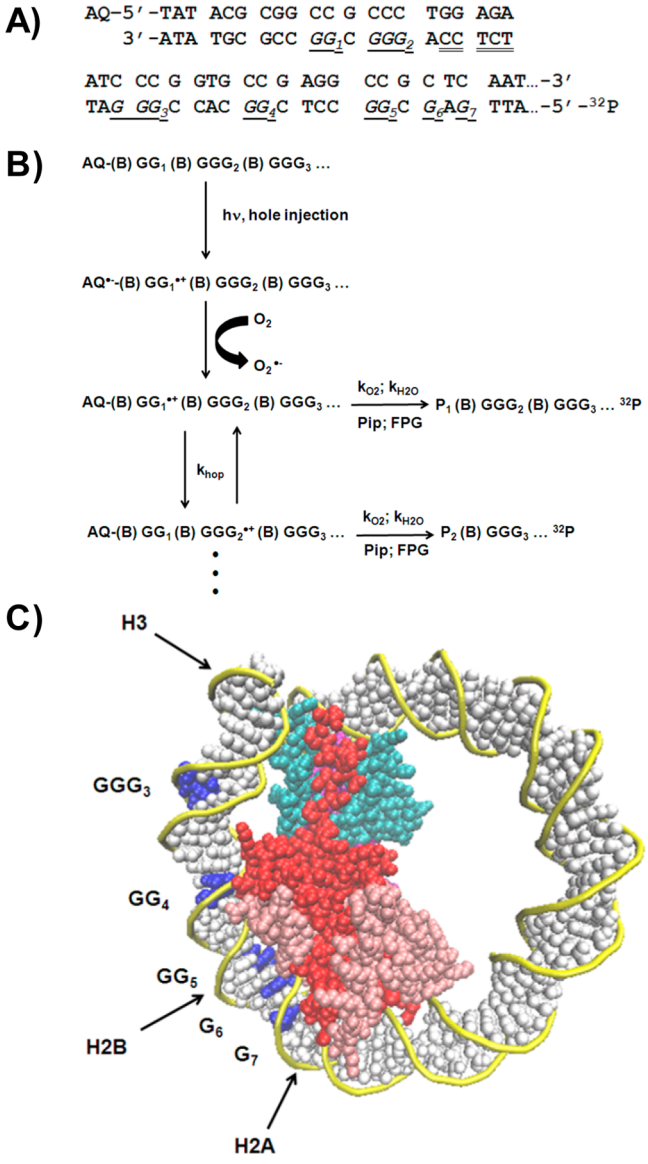

Figure 1. Overview of DNA HT in AQ-601 constructs. (A) Sequence of AQ-601 and the guanine oxidation sites observed in both naked and NCP constructs following DNA HT. The pyrimidine tract where DNA-H3 cross-linking occurs in the NCP is double-underlined. (B) Overview of HT dynamics in AQ-601. Following photoexcitation, an electron is transferred from site GG_1 to AQ over the intervening bridge (B). The resulting hole is liberated by removal of the electron from AQ by O_2, and the hole can either hop to the next guanine site with the rate k_{hop} or be trapped by O_2 (H_2O) with the rate k_{O_2} (k_{H_2O}) and treated with piperidine (FPG) to form the strand break products P_1, P_2, etc. (C) Structure of rAQ-601 constructed using the crystal structure of 601 NCP (Protein Data Bank entry 3LZ0) and previous DNA footprinting of rAQ-601. The linker DNA with the 5′-AQ photooxidant and sites GG_1 and GGG_2 is not shown. Only the copy of histone H2A (red), H2B (pink), H3 (cyan), and H4 (purple) closest to the AQ-601 HT region is shown for the sake of clarity. Also indicated by arrows are the approximate exit points of the histone H2A, H2B, and H3 N-terminal tails. The H3−DNA cross-link sites in rAQ-601 are in the region around the H3 arrow.

the folded core of the histone octamer, and the following local environment around each site is expected. At site GGG_3, the DNA minor groove is rotated away from the histone surface and there are no molecular contacts between any histone

dx.doi.org/10.1021/bi201734c | Biochemistry 2012, 51, 3129−3142

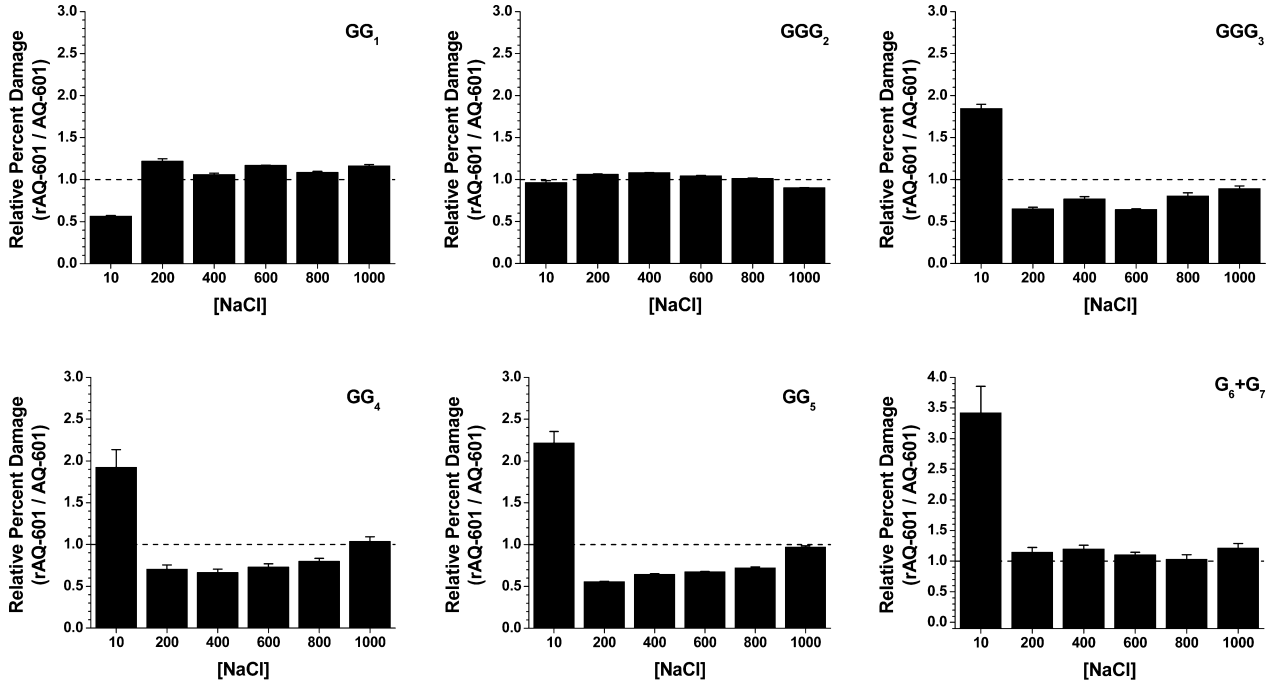

Figure 2. Salt dependence of the relative percent damage ratios measured at sites GGG_1–G_7 in naked AQ-601 and rAQ-601 following UV-A irradiation and hot piperidine treatment. A relative percent damage ratio greater than 1 indicates greater guanine damage observed in the NCP vs naked DNA. Note that the *Y* axis scale is increased for the G_6+G_7 site.

residues and the DNA nucleobases or backbone (distance of all atoms of >5 Å). Site GG_4 is in superhelical location −6 and has its minor groove rotated toward the histone core. The charged guanidinium side chain of H2B Arg77 makes contact with minor groove surfaces of both GG_4 guanine residues in the crystal structure, and it could potentially modulate DNA HT dynamics in the NCP because of its charged nature.[25,30] Site GG_5 has its minor groove rotated away from the histone surface, and the guanine backbone atoms are in contact with residues in histone H2B (Lys28–Lys31) adjacent to the point where the N-terminal tail of this histone exits the nucleosome. The minor groove of bases G_6 and G_7 is rotated toward the histone surface, and both residues make contact with histone proteins. In particular, the backbone of G_6 makes contact with several residues in H2B and H2A, while the side chain of H2B Arg30 is located in the minor groove near G_7.

Hole Transport Dynamics in AQ-601 and rAQ-601 Exhibit Different Dependencies on Salt. Following preparation, structural characterization, and UV-A irradiation, samples of naked or nucleosome-bound AQ-601 were treated with piperidine to generate strand breaks at the sites of oxidized guanines, and the products were quantified by autoradiography. At all salt concentrations, we observe seven sites of guanine oxidation in the UV-A-treated naked AQ-601 and rAQ-601 samples, but very minor background products in nonirradiated samples (Figure S3 of the Supporting Information). As discussed previously,[29] in the irradiated rAQ-601 samples there is an additional band (labeled XL in Figure S3 of the Supporting Information) located in the pyrimidine tract directly 5′ to site GGG_2. These lesions are due to a DNA HT-induced cross-linking reaction involving residue(s) in histone H3 (approximate location is near the H3 arrow in Figure 1C). Although the dynamics of DNA–histone cross-linking are not the focus of this work, we will periodically return to this side reaction to discuss its relationship to the guanine oxidation levels observed in rAQ-601.

To evaluate our data at each salt concentration, we first calculated the percent damage at the seven guanine oxidation sites at each salt concentration. To facilitate the analysis of the changes in guanine oxidation between naked and rNCP samples, we show in Figure 2 the ratio of percent damage between the rAQ-601 and naked AQ-601 samples (a ratio of 1 indicates that equal amounts of normalized damage products were observed at a specific guanine site in both samples). In this and all further data analysis steps, we have combined the damage at sites G_6 and G_7 together because (1) they are single guanines and their efficiency of oxidation is expected to be lower than at the GG and GGG sites and (2) they are the sites farthest from the AQ photooxidant and their relative amounts of damage are generally smaller than those of the other sites, especially in naked AQ-601. At 10 mM salt, we observe (i) a decrease in the relative amount of damage at site GG_1 in the NCP, (ii) no difference in normalized damage at GGG_2, and (iii) a significant increase in the level of damage at sites GGG_3–G_7 in the nucleosome. These data indicate that at 10 mM salt there is an enhancement of guanine oxidation at the nucleosome packaged sites (GGG_3–G_7) in rAQ-601 over their normalized oxidation efficiency measured in naked DNA. As the salt concentration increases, there are several different behaviors observed for the individual guanine oxidation sites, and we can break them up into four groups. (1) Site GG_1. As the salt concentration increases from 10 and 200 mM, the percent damage ratio at site GG_1 becomes nearly identical in the two DNA samples and remains identical up to 1000 mM. (2) Site GGG_2. The relative damage level observed at site GGG_2 is largely independent of salt and DNA packaging. (3) Sites GGG_3, GG_4, and GG_5. The percent damage ratios shift from an increased amount of damage in the NCP at 10 mM salt to significantly smaller amounts of damage in the NCP between

dx.doi.org/10.1021/bi201734c | *Biochemistry* 2012, 51, 3129–3142

200 and 800 mM NaCl. By 1000 mM salt, the percent damage ratio between AQ-601 and rAQ-601 is near 1, indicating that guanine oxidation distributions in naked and nucleosomal samples are nearly indistinguishable at high salt concentrations. (4) Site G_6+G_7. The damage ratio decreases sharply between 10 and 200 mM salt, but then the normalized amount of guanine damage measured in AQ-601 and rAQ-601 is virtually identical between 200 and 1000 mM NaCl. Overall, this analysis indicates that there is a clear enhancement of long-range guanine oxidation in the nucleosome at 10 mM salt, a sharp decrease in nucleosomal guanine oxidation at intermediate salt concentrations, and nearly identical guanine damage distributions in both samples at 1000 mM NaCl.

The strong variation in guanine damage distributions indicates that the DNA HT dynamics in AQ-601 change depending on the local environment. Normalized HT damage yields (ϕ) typically show a shallow exponential decrease as the distance between the donor and hole trapping site (R_{DA}) increases according to eq 1

$$\phi \propto \exp(-\beta R_{DA}) \quad (1)$$

where β is a phenomenological parameter loosely related to the electronic properties of the transport material (DNA). Changes in HT dynamics, due to DNA structure or environment, are expected to be exhibited as a variation in β. To compare and contrast the dynamics of DNA HT between AQ-601 and rAQ-601 at all salt concentrations, we transformed our guanine oxidation data to plot $\ln(G_x/GG_1)$ versus R_{DA} (Figure 3). The G_x/GG_1 ratio provides an estimate of the normalized guanine oxidation yield (ϕ), and its use is standard in the field of DNA HT. R_{DA} is the distance between AQ and the guanine oxidation sites, and it was calculated on the basis of a B-form DNA duplex (rise of 3.4 Å/bp). For GGG sites, we measured from AQ to the central G; for GG sites, we measured to the 5′-G, and for G_6+G_7 sites, we used the distance to the AT base pair between the two guanines. We used the same R_{DA} values for sites GGG_3−G_7 in AQ-601 and rAQ-601 because the simplified calculation based on 3.4 Å/bp results in a <2 Å difference from a sum of base pair rise values obtained from a 3DNA[43] analysis of the 601 crystal structure (Figure 1C).

Turning first to AQ-601 (Figure 3A), we will briefly reiterate the results we obtained in our previous report about the salt dependence of DNA HT in this construct.[34] First, at all salt concentrations, the G_x/GG_1 ratios decrease with an increasing R_{DA}, as expected from eq 1, but the plots are nonlinear with a break between GGG_2 and GGG_3. The nonlinearity is due to the fact that site GGG_2 always has the largest amount of damage in the AQ-601 construct, evidenced by a GGG_2/GG_1 ratio greater than 1 [$\ln(GGG_2/GG_1) > 0.1$]. If we focus solely on the distance dependence of HT for sites GGG_3−G_7, the measured β parameter is nearly identical at all six salt concentrations, with a value of 0.012 ± 0.03 Å^{-1}. Even though the distance dependence of DNA HT is independent of the concentration of salt, the efficiency of HT to sites GGG_2−G_7 is dependent on bulk salt concentration with an initial increase in long-range DNA HT as the salt goes from 10 to 200 mM, followed by a decrease in transport efficiency with increasing salt concentration.

The transport dynamics in rAQ-601 are shown in Figure 3B, and the first thing that stands out in these data is the reinforcement of the fact that HT is maximal at 10 mM NaCl in the nucleosome, not at 200 mM salt as for AQ-601. Also surprising is the near lack of distance dependence ($\beta \sim 0$ Å^{-1})

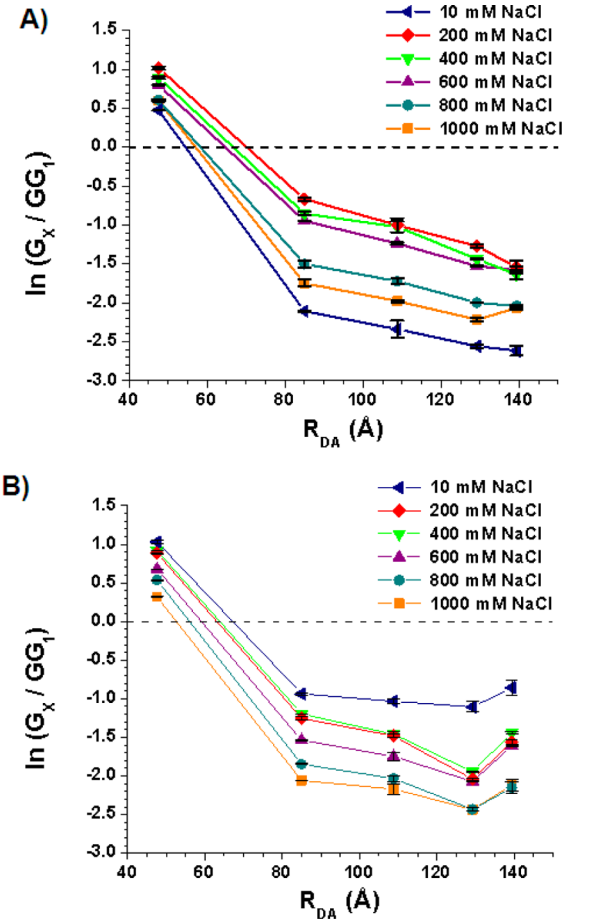

Figure 3. Comparison of the normalized damage ratios (G_x/GG_1) in naked AQ-601 (A) and rAQ-601 (B) as a function of salt concentration. The points on each curve, from left to right, are the ratios measured at sites GGG_2, GGG_3, GG_4, GG_5, and G_6+G_7, respectively.

for transport between GGG_3−G_7 sites at 10 mM salt in the nucleosome. The data in Figures 2 and 3B clearly indicate that there are significant environmental changes in the NCP that enhance long-range HT at low salt concentrations. As the salt concentration increases, DNA HT efficiency in the nucleosome becomes progressively lower because the G_x/GG_1 ratios decrease. Between 200 and 1000 mM NaCl, the β values measured for transport to sites GGG_3 and GG_5 are indistinguishable from the β values calculated in AQ-601. Therefore, the dynamics of HT in AQ-601 and rAQ-601 between 200 and 800 mM are similar, even though the relative levels of guanine oxidation at sites GGG_3−G_7 are higher in naked AQ-601 than in the NCP (Figure 2). By 1000 mM NaCl, both the dynamics of HT and the overall distribution of guanine oxidation at sites GGG_3−G_7 are essentially identical. Later in this work, we will provide a model based on the presence of the H3−DNA cross-links in rAQ-601 that describes the origin of these observations (see the next section and Discussion).

The Salt Dependence of DNA−H3 Cross-Linking in rAQ-601 Mirrors That Observed for Guanine Oxidation. Although it is not the primary focus of this work, we will briefly analyze how the salt concentration affects the amount of DNA−histone cross-linking in rAQ-601.[29] As we show below, the rationale for including these data is that it allows us to draw

dx.doi.org/10.1021/bi201734c | Biochemistry 2012, 51, 3129−3142

two important conclusions about DNA HT dynamics in rAQ-601. These cross-links arise from an off-pathway reaction between residues in H3 (presumably Tyr41) and pyrimidine residues located between GGG_2 and GGG_3 (Figure 1A). In our autoradiographs (Figure S3 of the Supporting Information), we first note that at all salt concentrations there is a cross-link band present just below GGG_2. Therefore, the first important insight provided by the presence of the DNA−H3 cross-link is that there is molecular contact between the 601 HT region and the folded core of histone H3 in rAQ-601 at all studied salt concentrations. Further, the similarity of DNA HT in rAQ-601 and naked AQ-601 at higher salt concentrations cannot simply be due to the complete disruption of DNA−histone interactions. Next, we quantified the relative level of cross-linking in rAQ-601 [percent damage (Figure 4A)] by dividing

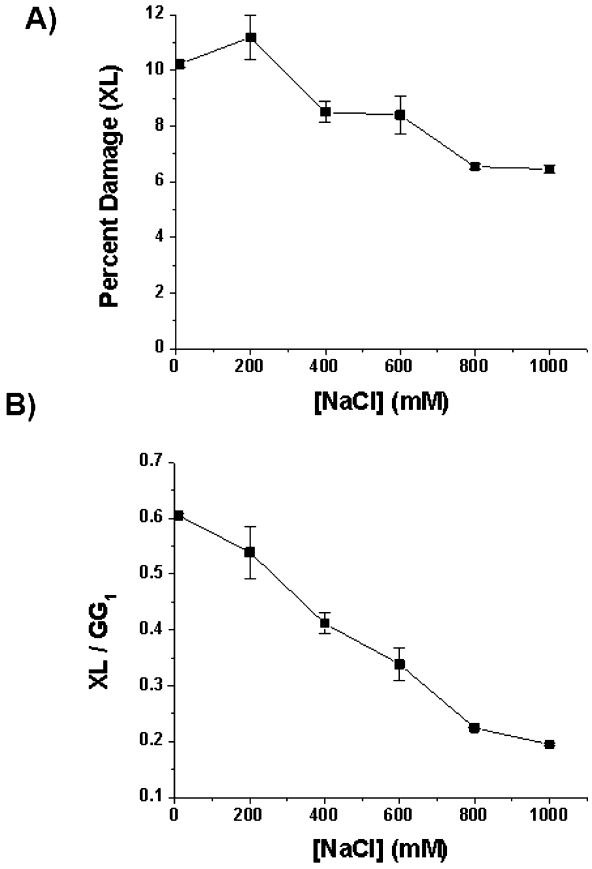

Figure 4. Influence of bulk salt concentration on the DNA−H3 cross-linking reaction (XL) in rAQ-601. (A) The percent damage of cross-linking remains constant between 10 and 200 mM NaCl but then decreases as the salt concentration increases. (B) As the NaCl concentration increases, the ratio of the damage at the XL site versus GG_1 decreases. The presence of DNA−H3 cross-linking at all salt concentrations indicates that the first turn of the AQ-601 sequence is in contact with the folded H3 core under all of the experimental conditions studied.

the intensity of the cross-link band by the sum of damage intensity at all guanine sites and the cross-link. Simultaneously, we calculated the ratio of the intensity of the cross-link band to that obtained for GG_1 (XL/GG_1) at all salt concentrations (Figure 4B). From these two related sets of data, it is clear that as the salt concentration increases, the amount of DNA−H3 cross-linking decreases. In fact, the decrease in cross-linking efficiency as the salt concentration increases mirrors the decrease in the level of guanine oxidation at the nucleosome-packaged sites (GGG_3−G_7) over this salt range. For example, the GGG_3/GG_1 ratio decreases by a factor of 3.1 between 10 and 1000 mM salt, while the XL/GG_1 ratio decreases by a factor of 3.0. Because all processes associated with DNA oxidation in rAQ-601, including both cross-linking and guanine oxidative damage, have a similar salt dependence, then the second important conclusion we draw from this section is that long-range DNA HT must be sensitive to changes in the local DNA environment affected by the perturbation of nucleosomal structure.

Removal of the Histone Tails from the AQ-601 Nucleosome Leads to DNA HT Dynamics Similar to Those of Naked DNA at Low Salt Concentrations. In the previous sections, we used increasing salt concentrations to disrupt the structure of the nucleosome and observed that HT dynamics become similar to those in naked DNA as the salt concentration increases and DNA−protein interactions are disrupted. We next sought a second, controlled way to perturb nucleosome structure that does not affect the bulk electrostatic properties of the surrounding environment (e.g., ionic strength). From previous studies, it is known that controlled trypsin digestion will remove the N- and C-terminal tails of the core histones but leave the folded core of the octamer intact to associate with packaged DNA.[44−46] In particular, trypsinization of the nucleosome leaves behind an octamer consisting of histones H2A(12−118), H2B(21−122), H3(27−129), and H4(20−102). The removal of the histone tails leads to destabilization of the nucleosome at 10 mM NaCl,[47,48] the salt concentration at which the effect of NCP packaging on DNA HT in AQ-601 was maximal. Therefore, we reconstituted AQ-601 onto trypsinized histones (trAQ-601) to investigate the effect that removal of the histone tails would have on DNA HT at 10 mM NaCl. Before conducting the HT assays, we first verified that the tailless NCPs had a mobility intermediate between those of AQ-601 and rAQ-601 on EMSA gels (Figure S2 of the Supporting Information). Samples of trAQ-601 and rAQ-601 were irradiated at the same time and worked up in an identical fashion to ensure that changes in the guanine oxidation data in the two samples were due solely to the absence of the histone tails. Figure 5 shows a comparison between the percent damage observed at all guanine sites in naked AQ-601, rAQ-601, and trAQ-601 at 10 mM NaCl obtained from autoradiography of sequencing gels (Figure S4 of the Supporting Information). The striking feature of Figure 5

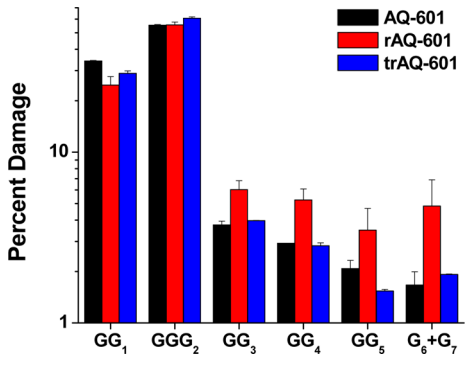

Figure 5. Comparison of the relative levels of guanine damage (percent damage) in AQ-601, rAQ-601, and trAQ-601 at 10 mM NaCl.

dx.doi.org/10.1021/bi201734c | *Biochemistry* 2012, 51, 3129−3142

is how the removal of the histone tails leads to DNA HT dynamics virtually indistinguishable from those in naked DNA at 10 mM NaCl. Also clear is the fact that at this salt concentration there are distinct differences in the distribution of guanine oxidative damage between AQ-601/trAQ-601 and the native rAQ-601 samples within the histone contact region (GGG_3–G_7). This experiment reinforces our earlier conclusion that there are distinct features of the native nucleosome environment that enhance long-range DNA HT at low salt concentrations, and it pinpoints the origin of this effect to the histone tails. We also note that the trAQ-601 samples still show the DNA–H3 cross-link product in the pyrimidine region between GGG_2 and GGG_3 (Figure S4 of the Supporting Information), a result that indicates that (1) the DNA near the NCP entrance in trAQ-601 maintains contact with the folded histone core at 10 mM NaCl and (2) the histone tails are not involved in the cross-linking reaction.

Nucleosomal Packaging Changes the Chemical Nature of the Guanine Lesions Arising from DNA HT. When guanine is oxidized during HT to form the guanine radical cation ($G^{\bullet+}$), there are two classes of chemical reactions that result in hole trapping, and each has its own distinctive spectrum of guanine oxidation products. In the first pathway, $G^{\bullet+}$ reacts with water to form $2e^-$ oxidation products like 8-oxoguanine (8OG).[49,50] The second pathway involves reaction of superoxide with $G^{\bullet+}$ to form $4e^-$ ring-opened lesions such as oxazolone (Oz).[51,52] Different assays can be used to quantify the relative yields of these classes of guanine-derived lesions in oxidized DNA. The first treatment, and the one we have used thus far in our experiments, is hot piperidine. Piperidine treatment leads to the formation of single-strand breaks at the sites of Oz, but not 8OG.[53] Enzymatic digestion using FPG is the second treatment, and it results in strand breaks at the sites of both 8OG and Oz.[54] Prior work has used the ratio of the yield of piperidine-labile lesions (Y_{pip}) to the yield of lesions susceptible to FPG (Y_{FPG}) to interrogate the local environment of guanine residues in DNA.[55,56] For instance, a Y_{pip}/Y_{FPG} ratio of >1 indicates that a guanine is in either a single strand or a weakly stacked double-strand region, whereas a Y_{pip}/Y_{FPG} ratio of <1 is observed for most guanines in B-form DNA duplexes.[55,56] Prior experiments examining photoinduced DNA HT in short, double-stranded, and single-stranded oligonucleotides have produced Y_{pip}/Y_{FPG} values consistent with this interpretation.[57,58]

To see if the packaging of DNA into a nucleosome affects the chemical nature of the guanine lesions in AQ-601, we performed assays in which the yields of piperidine-sensitive and FPG-sensitive guanine products were quantified side by side from UV-A-irradiated samples of naked AQ-601, rAQ-601, and trAQ-601 (Figure S4 of the Supporting Information). These assays were all conducted in 10 mM NaCl buffer because the NCP is the most stable at this low salt concentration, and this was the salt concentration that showed the largest difference between naked and nucleosomal HT dynamics. Figure 6A shows a log–linear plot of the percent damage observed at sites GG_1–G_7 in the three AQ-601 samples after piperidine or FPG treatment. The piperidine data in Figure 6A reinforce the trends presented in Figure 5; the damage distributions in AQ-601 and trAQ-601 look nearly identical, while the relative damage levels at the NCP packaged sites in rAQ-601 are higher. In AQ-601 and trAQ-601, the FPG damage distributions are nearly identical to those obtained using piperidine, except at site G_6+G_7. The FPG-sensitive

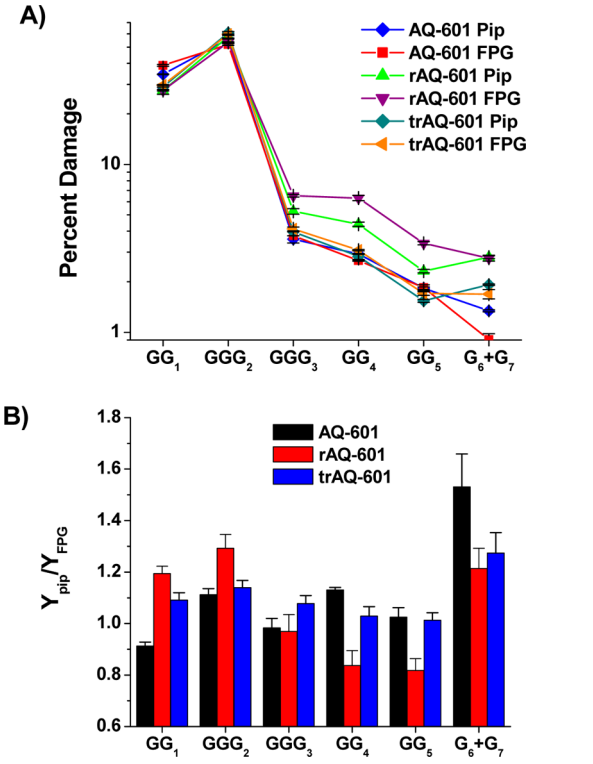

Figure 6. Comparison of the yields of piperidine- and FPG-sensitive guanine oxidative lesions at sites GG_1–G_7 in naked AQ-601, rAQ-601, and trAQ-601 at 10 mM NaCl. (A) Percent damage values for the three samples arising from either piperidine or FPG treatment. (B) Ratio of piperidine to FPG damage yields (Y_{pip}/Y_{FPG}).

damage in rAQ-601 in the nucleosome-packaged region is higher than that observed for FPG-treated AQ-601 or trAQ-601. In addition, the relative FPG damage levels at sites GGG_3–GG_5 in rAQ-601 are higher than the piperidine values measured in this same construct. In summary, Figure 6A shows that the efficiency of generating both piperidine- and FPG-sensitive damage at the guanine sites farthest from the AQ photooxidant is maximal in the nucleosome with the native histone proteins, and that histone tail removal results in a reduction in the level of both piperidine- and FPG-sensitive guanine lesions. Furthermore, Figure 6A indicates the distribution of piperidine- and FPG-sensitive lesions is similar in AQ-601 and trAQ-601, but there are differences in the guanine oxidation products in rAQ-601.

We next calculated the Y_{pip}/Y_{FPG} ratio for all of the guanine sites in the three constructs using the methodology outlined in Experimental Procedures (Figure 6B). At most sites in naked AQ-601, $Y_{pip}/Y_{FPG} = 1 \pm 0.1$ except at GG_4 (slightly above 1.1) and G_6+G_7 (~1.55). The ratios measured at sites GG_1–GG_5 are larger than those typically observed for guanine multiplets in shorter DNA duplexes ($0.4 \leq Y_{pip}/Y_{FPG} \leq 0.8$),[56] indicating that base pair stacking at these sites in naked AQ-601 at 10 mM salt is expected to be slightly weaker than for a "typical" GG or GGG site. The high Y_{pip}/Y_{FPG} ratio at site G_6+G_7 is similar to values observed at poorly stacked single-guanine sites in short DNA duplexes. These data indicate that this region of 601 DNA deviates in subtle ways from a regular B-form structure. Given that underwinding (less base pair stacking) is an inherent property of DNA packaged into the nucleosome, these observations may provide a deeper understanding of why the 601 sequence forms NCPs of high thermodynamic stability.

dx.doi.org/10.1021/bi201734c | *Biochemistry* 2012, 51, 3129–3142

Further, it complements our previous observation that the 601 sequence has the unusual property of becoming further underwound as the salt concentration increases.[34]

Once the nucleosomes are packaged into the NCP (rAQ-601), the Y_{pip}/Y_{FPG} ratios for sites in the linker region (GG_1 and GGG_2) significantly increase at 10 mM salt. This is in contrast to the behavior of the histone-associated sites GGG_3−G_7, where the Y_{pip}/Y_{FPG} ratios are nearly identical at site GGG_3 for nucleosome versus naked DNA, and the ratio is significantly decreased in the nucleosome at the distal guanine oxidation sites. This result indicates that there is a shift from a slight propensity to form piperidine-sensitive lesions in linker DNA to a propensity to form FPG-sensitive lesions in the packaged DNA region. The most straightforward explanation for these results is DNA packaging into the NCP results in the favoring of the $2e^-$ $G^{\bullet+}$ trapping reactions involving H_2O over the $4e^-$ processes involving O_2. Because both the H_2O and O_2 reactions arise from the same kinetic intermediate, $G^{\bullet+}$, the shift in the guanine oxidation product distribution is most likely due to a change in the ratio of trapping rates, k_{O_2}/k_{H_2O} (Figure 1B). As discussed in the previous paragraph, the typical approach to explaining how environmental changes lead to decreases in Y_{pip}/Y_{FPG} ratios relies on the interpretation that an increased level of guanine base stacking reduces the accessibility of $G^{\bullet+}$ to O_2 (i.e., reduced k_{O_2}). To see if there is any evidence of an increased level of stacking in the NCP versus naked AQ-601, we used 3DNA[43] to analyze the structure of sites GGG_3−GG_5 in the 601 NCP crystal structure (Figure 1C). As a snapshot of the guanine stacking interactions at these sites, we present the values of the base step parameters rise and twist at the four 5′-GG-3′ steps (GGG_3-1 refers to the 5′ and central G of the triplet, and GGG_3-2 refers to the central and 3′-G of the triplet) in Table 1. The values of the parameter rise for steps GG_4 and GG_5 are nearly the same as for B-form DNA (3.4 Å), whereas the values for GGG_3-1 and GGG_3-2 are smaller. For twist, the values for GGG_3-1, GGG_3-2, and GG_5 are all similar, but GG_4 has a significantly higher twist value. This large twist value in GG_4 leads to virtual unstacking of the two guanines at this site in the NCP. To quantify how large the unstacking effect at GG_4 is, we also present in Table 1 the overlap stacking area for each GG pair. These data show that for GG_4, the base overlap is lower by a factor of 6−7 as compared to the values of the three other GG steps. Even though we do not have an experimental snapshot of the ensemble structure surrounding GG_4 in naked AQ-601 at 10 mM salt, we can use the results of our previously reported 10 ns molecular dynamics simulation on a decamer containing the GG_4 region of AQ-601.[34] The average values of rise, twist, and base overlap area from this simulation are listed in Table 1. Clearly, the loss of guanine stacking at GG_4 in the NCP is counter to the expectation of an increased level of stacking (decreased Y_{pip}/Y_{FPG} ratio) at this site in the nucleosome.

Table 1. Values of Base Pair Parameters for the GG Steps in Sites GGG_3−GG_5 Calculated from the NCP Crystal Structure (Figure 1) Using 3DNA[43]

GG step	rise (Å)	twist (deg)	stacking area (Å^2)
GGG_3-1	3.10	30.5	4.0
GGG_3-2	2.78	33.1	4.12
GG_4	3.52	48.7	0.65
GG_4*[a]	3.46	34.5	4.45
GG_5	3.47	33.3	4.74

[a]The values for GG_4* are average values obtained from our previous NPT molecular dynamics simulation of a GG_4-containing dodecamer at 100 mM NaCl.[34]

The final piece of evidence against changes in DNA secondary structure controlling the Y_{pip}/Y_{FPG} ratio comes from the data obtained from trAQ-601. In the DNA linker region, the loss of the histone tails results in a decrease in the Y_{pip}/Y_{FPG} ratio in the nucleosome samples, and tail removal results in a loss of the preference for FPG-sensitive lesions in the nucleosome at sites GGG_3−GG_5 as evidenced by increased Y_{pip}/Y_{FPG} ratios at these sites in trAQ-601 versus rAQ-601. DNA−H3 cross-linking is observed in both rAQ-601 and trAQ-601, so the DNA in both systems must be in contact with the folded histone core; presumably the DNA structure in both samples is similar. Therefore, the most likely explanation for these experimental results is the histone tails at 10 mM salt modulate the reaction of $G^{\bullet+}$ with O_2, in both the linker DNA (sites GG_1 and GGG_2) and the histone-associated region (sites GG_4−G_7).

DISCUSSION

In the experiments reported here, we have systematically applied several levels of perturbation to the AQ-601 DNA hole transport system. Previously, a combined experimental and theoretical analysis of the salt dependence of HT in naked AQ-601 led to the conclusion that the dynamics were controlled by the rates of hole trapping, and not the rates of hole hopping between the observable guanine oxidation sites.[34] This conclusion was reached by (i) showing that changing the concentration of bulk salt is not expected to lead to large changes in the structural fluctuations that control guanine oxidation potentials (related to hole hopping rates)[9,59−63] and (ii) the observation that the salt dependence of long-range transport most closely follows the known effects of salt on the diffusion rates of O_2 species in aqueous media,[64,65] a process that will control the rate at which piperidine-sensitive lesions are formed at oxidized guanines.[49−51]

The first perturbation we applied to AQ-601 was to wrap this sequence around the histone octamer to form a NCP. From the data in Figures 2−4, there are clearly different effects of DNA packaging on HT dynamics at very low salt (10 mM) versus the higher salt concentrations (200−1000 mM). At 10 mM salt, there is an enhancement of long-range DNA HT to the guanine sites in contact with the nucleosome surface (GGG_3−G_7); however, between 200 and 1000 mM salt, the relative levels of damage at the distal guanine sites are higher in AQ-601 than in rAQ-601. The second perturbation we applied was to remove the N-terminal tails of the core histones and then interrogate DNA HT at 10 mM salt, the concentration with the most dramatic difference between naked and nucleosomal DNA. Surprisingly, the removal of the histone tails from the AQ-601 nucleosome is sufficient to eliminate the effects of nucleosomal packaging on long-range DNA HT, even though the DNA is still in contact with the folded core domains of the histones. Clearly, to interpret the effects of nucleosome packaging on DNA HT, we need to compare and contrast the changes in the DNA HT to the known effects of changes in ionic strength and histone tail removal on the structure and biophysical dynamics of mononucleosomes.

The first property of NCPs critical for our analysis of DNA HT is the effect of salt on mononucleosomes. There are two major structural changes that occur in NCPs as the salt

dx.doi.org/10.1021/bi201734c | Biochemistry 2012, 51, 3129−3142

concentration increases: (1) The level of DNA breathing near the entrance and exit points of the NCP increases, and (2) there is selective loss of histone proteins. DNA breathing is characterized by spontaneous structural fluctuations leading to the reversible unwrapping and wrapping of DNA from the histone core, even at low salt concentrations where the NCP has maximal thermodynamic stability.[66−68] Because of the high thermodynamic stability of the 601 nucleosome, at 10 mM salt there is contact between 90 and 98% of the DNA ends (first 10 bp) and the octamer surface at any given time. The lifetime of the 601 wrapped state at low salt is 250 ms, and the unwrapped state lasts for 10−50 ms.[66] Because the lifetime of the wrapped state is longer than the lifetimes previously measured for either guanine hole hopping (nanoseconds to microseconds) or hole trapping reactions (microseconds), the entire HT process from photoinitiation to trapped guanine lesion in rAQ-601 is expected to take place predominantly in a fully wrapped structure at 10 mM NaCl. Our footprinting studies with rAQ-601 provide further evidence of the predominance of the wrapped DNA state in our construct at 10 mM NaCl.[29] As the salt concentration increases, the equilibrium shifts toward the solvent-exposed, unwrapped state, and 600 mM NaCl is the concentration at which the equilibrium constant approaches 1 (50% of DNA ends wrapped). In addition to changes in DNA−protein interactions, there are also changes in protein−protein interactions in the histone core that occur as the salt concentration increases. The coupled FRET and fluorescence anisotropy measurements of Hoch et al.[38] showed that below 600 mM salt the histone octamer in 601 NCPs is intact, but between 700 and 1500 mM the structure is dominated by mixed species consisting of 601 DNA wrapped around either just the H3−H4 tetramer or a hexameric intermediate consisting of the H3−H4 tetramer and one H2A−H2B dimer.

In addition to the previously described interactions between DNA and the folded histone core, the lysine and arginine rich histone tails also play a role in NCP stability. At low salt concentrations, the basic N-terminal tails of H2A, H2B, and H3, but not H4, are in molecular contact with the packaged DNA in a mononucleosome, but they dissociate as the salt concentration increases because of electrostatic screening.[39,69] With respect to the H3 N-terminal tail, ^{13}C NMR experiments,[70] radiolabeling reactions,[71] and enzymatic modification[72] have shown that this tail makes contact with linker DNA at low salt concentrations,[73−75] with some residues even folding into an α-helical structure upon DNA binding.[76] Photochemical cross-linking reactions have shown that the H2A tail interacts with DNA ~30 bp from entrance to NCP,[77] while enzymatic reactions have indicated that H2B interacts with DNA near the point where its N-terminal tail exits the NCP.[75] As an alternative to increasing ionic strength, the removal of the histone tails through limited proteolysis is a classic technique used to study nucleosome stability and structural dynamics. NCPs that have their tails removed display anomalous behavior at low salt concentrations; for instance, tailless NCPs have a much larger radius of gyration than intact NCPs at 10 mM NaCl, and the tailless system becomes more compact as the salt concentration is increased from 10 to 50 mM NaCl.[47] Further, Polach et al.[48] showed that there is a slight increase in the population of unwrapped 601 DNA at the entrance of tailless NCPs at low salt concentrations.

With this brief introduction to nucleosome structural dynamics, we will now apply this information to gain a detailed understanding of our nucleosomal AQ-601 HT data. Our working hypothesis for the rest of this discussion will be that any changes in DNA HT dynamics in rAQ-601 or trAQ-601 are due to perturbations of hole trapping rates by DNA−protein interactions. We will start with a comparison of the 200−1000 mM NaCl data for AQ-601 and rAQ-601 from Figures 2 and 3. At first glance, it is tempting to ascribe the decrease in the level of long-range HT with an increasing salt concentration in rAQ-601 to (i) an increased level of DNA breathing, which leads to (ii) higher DNA solvent accessibility, (iii) increased hole trapping rates, and thus (iv) a lower efficiency of long-range HT. This hypothesis is not supported by the experimental data because even though the relative amount of HT damage at sites GGG_3−G_7 decreases with an increasing salt concentration, the G_x/GG_1 ratios in AQ-601 are larger than those measured in rAQ-601, especially at sites GGG_3−GG_5 and salt concentrations between 200 and 800 mM (Figure 3). Using our working hypothesis that hole trapping reactions control the final guanine damage distributions in both AQ-601 and rAQ-601, it is difficult to rationalize a realistic model in which the hole trapping rates would be faster in DNA packaged in the nucleosome versus free in solution. An alternative explanation for the HT data in AQ-601 and rAQ-601 over this range of salt concentrations is that the hole transport dynamics are identical in the two systems between 200 and 1000 mM NaCl except for the presence of the competing DNA−H3 cross-linking reaction in the nucleosome. A simple kinetic model (Figure 7) can be used to show that the presence of the DNA−H3 cross-linking reaction can lead to lower G_x/GG_1 ratios in rAQ-601 than in AQ-601. In this model, there are five guanine oxidation sites, and holes hop forward and backward with rates k_F and k_B, respectively. Side reactions lead to hole trapping products (P_i; rate of k_T), and there is a side reaction from site G_2 that leads to

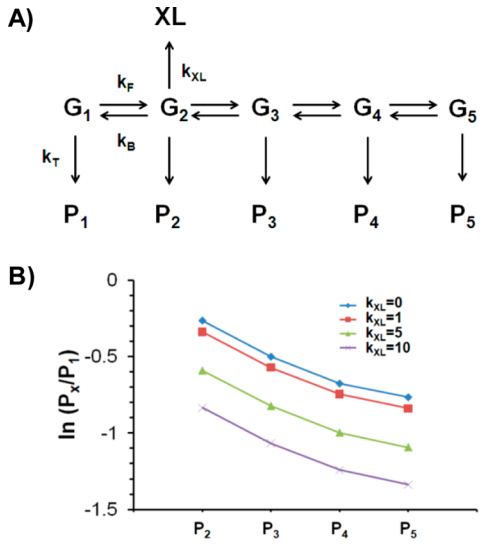

Figure 7. Simple kinetic model of DNA HT with an off-pathway DNA−histone cross-linking reaction that can be used to explain the lower efficiency of long-range DNA HT in NCP-packaged AQ-601 between 200 and 800 mM NaCl. (A) Kinetic model for DNA HT in a system with five observable guanine damage sites. k_F and k_B are forward and backward hole hopping rates; k_T is the rate of hole trapping, and k_{XL} is the rate of cross-linking near site G_2. At time zero, $[G_1] = 1.0$ and all others are zero. (B) Calculated P_i/P_1 ratios decrease as the rate of DNA−protein cross-linking (k_{XL}) increases. For each curve, the coupled kinetic equations were numerically integrated using $k_F = k_B = 10$, $k_T = 1$, and the indicated value of k_{XL}.

dx.doi.org/10.1021/bi201734c | *Biochemistry* 2012, 51, 3129−3142

cross-linking (k_{XL}). To model HT, we set $[G_1]$ equal to 1 at time zero and used Scilab to numerically integrate the coupled kinetic equations. In all cases, we set $k_F = k_B = 10k_T$ on the basis of previous DNA HT models of systems with mixed AT bridges between guanine sites.[15] As shown in Figure 7B, as the amount of cross-linking increases (larger k_{XL}), the P_i/P_1 values are expected to decrease. Although this model is clearly an oversimplification of the 601 transport sequence, it does explain our salt-dependent transport data. At 200 mM salt, where the H3−DNA cross-linking reaction is most efficient (Figure 4), the G_x/GG_1 ratios are lower in rAQ-601 than in AQ-601 (compare data in panels A and B of Figure 3). At the highest salt concentrationo (1000 mM), the efficiency of cross-linking is lower and the G_x/GG_1 ratios in the two systems become more identical (Figure 3). A more detailed model would be necessary to account for differences at the individual guanine sites in AQ-601, especially the insensitivity of sites GGG_2 and G_6+G_7 to nucleosomal packaging (Figure 2). The conclusion to be drawn from this part of our analysis is that DNA HT in rAQ-601 is largely insensitive to the known structural changes in the NCP that occur over the 200−1000 mM NaCl range. For example, we do not observe any sharp changes in DNA HT in rAQ-601 between 600 and 1000 mM NaCl that are not mirrored in the data for naked AQ-601 over this range (compare data in panels A and B of Figure 3). This is in spite of the expectation of the loss of DNA−protein contacts at sites GG_4−G_7 as the H2A−H2B dimers dissociate.[38] The important conclusion to draw from this analysis is that even when DNA is associated with proteins like the histone octamer, and there are known perturbations to DNA structure and environment, there may be little to no discernible change in the spectrum of guanine damage that arises from HT.

In contrast to the data at high salt concentrations, the DNA HT dynamics observed at 10 mM NaCl are clearly different in rAQ-601 and naked AQ-601. Further, the influence of DNA−H3 cross-linking on the guanine oxidation ratios (Figure 7) is not capable of explaining the increase in the G_x/GG_1 ratio (and percent damage) at sites GGG_3−G_7 in the nucleosome. Because the histone tails contact NCP-packaged DNA at low salt concentrations but then dissociate at high salt concentrations, we next tested the hypothesis that it was association of the histone tails with AQ-601 at 10 mM salt that leads to enhanced DNA HT. Indeed, the reconstitution of AQ-601 onto tailless histone proteins leads to DNA HT dynamics that are very similar to those in naked AQ-601. We exclude DNA sliding on the surface of the nucleosome as an alternative explanation for the similarity of DNA HT in naked AQ-601 and trAQ-601 because changes in nucleosome positioning are typically observed only in longer DNA constructs (>200 bp) with weak binding sequences like 5S rDNA.[78] The similarity of the HT dynamics in AQ-601 and rAQ-601 at 200−1000 mM is consistent with electrostatic screening leading to dissociation of the histone tails from the 601 DNA between 10 and 200 mM NaCl. Because the tails play a large role in controlling DNA HT in the NCP, the next question is which tails are important. The proteolysis of all four histones via trypsinization does not allow us to address the individual histone tails, but we suspect that the H2A, H2B, and H3 tails are all involved because (1) site GG_5 is near the exit point of the H2B N-terminal tail and GG_4 is a half-helical turn away from this position, (2) G_6 and G_7 are in the region where the H2A tail emerges from the NCP, and (3) GGG_3 is a half-helical turn from the exit point of the H3 N-terminal tail. Because a stochastic distribution of DNA−histone tail interactions is most likely responsible for the perturbation of DNA HT at 10 mM salt, molecular details will have to come from simulations or NMR spectroscopy.

Because the histone tails strongly affect the HT dynamics in rAQ-601, the next question revolved around whether the association of the tails in the nucleosome led to changes in the hole hopping or trapping rates. Strong evidence of the modulation of the hole trapping reactions in rAQ-601 comes from our analysis of the chemical nature of the guanine lesions generated from HT. The use of both piperidine and FPG on identically treated samples has allowed us to perform the first exploration of how DNA packaging affects the nature of the guanine lesions that arise from DNA HT in chromatin. In particular, treatment of identically prepared samples with either piperidine or FPG delineates the relative propensity of guanine radical cations to react with either oxygen species or water to form lesions like Oz or 8OG, respectively.[17,54] The observation that at 10 mM salt the ratios of piperidine to FPG-sensitive lesions at most guanine sites in naked AQ-601 and trAQ-601 are very similar indicates that the relative kinetics of the charge trapping reactions are similar in these two constructs. The shift away from piperidine lesions (e.g., Oz) to FPG lesions (e.g., 8OG) at sites GG_4−G_7 in rAQ-601, and the concomitant opposing shift toward piperidine-sensitive lesions in the linker region, indicate that there are changes in the hole trapping dynamics once the DNA is wrapped around the histone core and associates with the tails. While our data are not sufficiently comprehensive to allow us to definitively state whether the rate of reaction of $G^{\bullet+}$ with either H_2O or O_2 (or perhaps both) is affected by contact with the histone tails, we favor the hypothesis that there is a significant decrease in the rate of reaction of $G^{\bullet+}$ with oxygen species, and therefore an indirect increase in the amount of FPG-sensitive lesions arising from H_2O reactions. This hypothesis is consistent with previous studies showing that steric hindrance protects NCP-packaged DNA from attack by other diffusible species like hydroxyl radicals and DNA-methylating agents.[79−81]

Evidence against hole hopping rates controlling DNA HT dynamics in the nucleosome comes from the expected unstacking of GG_4 in the NCP (Table 1). Prior theoretical analyses of DNA HT have concluded that structural fluctuations in DNA can control hole transport by modulating both the relative oxidation potentials of guanine residues and the electronic coupling between oxidation sites via changes in base pairing and base stacking interactions (predominantly changes in twist and rise). We previously analyzed the effect of NCP packaging on guanine oxidation potentials in the human α-satellite DNA nucleosome,[30] a sequence that had a GG step at the same location as GG_4. Our calculations showed that this particular GG step is expected to be significantly harder to oxidize (and thus display reduced hole hopping rates) than GG steps located in other regions of the NCP. These structural considerations imply that if hole hopping rates were controlling the overall HT dynamics in rAQ-601, then we would expect to see a dramatic decrease in transport efficiency to sites GG_4−G_7 in the NCP because of the disruption of the DNA π-stack at site GG_4. Once again, the modulation of hole trapping rates but not those of hole hopping remains the best framework for interpreting our experimental results.

The results of this study allow us to look at previous work in the field of protein-packaged DNA in a new light. First, the observation that nucleosome packaging can perturb DNA HT in a salt concentration-dependent manner explains the

differences between the prior studies of Nunez and Barton,[27] who reported that DNA HT was unaffected by nucleosome packaging, and Bjorklund and Davis, who reported subtle but reproducible decreases in the level of long-range guanine oxidation in the NCP.[28] In the study by Nunez et al., the final step in NCP reconstitution was dialysis against TE buffer with no added salt. Prior work[82] on NCPs in TE buffer has shown that as the ionic strength of the solution decreases, the NCP's radius of gyration increases just like after histone tail removal. Therefore, there is consistency between the findings that DNA HT is equivalent in naked DNA and tailless NCPs in this study, and the observation that DNA HT in naked DNA and NCPs in low-salt TE is equivalent in the prior work of Nunez et al. Our other study[28] of DNA HT in the nucleosome utilized TG motif DNA (construct AQ-157TG), a sequence that reconstitutes to form a nucleosome with a stability lower than that of 601. In this previous work, we observed that there was a decrease in the level of long-range guanine oxidation at 10 mM NaCl in the NCP versus naked DNA, and we observed that histone tail removal in this system had a minimal effect on long-range DNA HT. Because the TG motif forms mononucleosomes with a stability lower than that of 601 DNA, the tails in the former NCPs may not be associated with the packaged DNA at 10 mM salt. This would lead to similar DNA HT dynamics in the tailless and native histone NCPs. We also note that the TG motif NCPs showed a large decrease in the levels of guanine oxidation as compared to the naked AQ-157TG. From the 200−1000 mM data for AQ-601 and rAQ-601, we would expect the formation of the H3−pyrimidine cross-links in the AQ-157TG NCPs to lead to a decrease in hole transport efficiency to the guanine sites farthest from AQ, just as was observed. In summary, the salt-dependent DNA HT dynamics in rAQ-601 allow us to provide a detailed framework for understanding all previously reported studies of DNA HT dynamics in the nucleosome core particle.

The only other set of DNA HT studies that reported an increase in the level of long-range DNA HT upon protein binding was the work of Rajski and Barton[22] utilizing either the antennapedia homeodomain protein or *Pvu*II restriction endonuclease. In both cases, there was an enhancement of HT to a distal GG site in the DNA−protein complex at very low ionic strengths, a dynamic similar to our results for rAQ-601 at low salt concentrations. The authors of this previous study attributed the effects of protein binding to changes in processes expected to impact hole hopping rates. However, because the authors used mixed sequence DNA constructs, much like AQ-601, their experiments may instead be reflecting changes in hole trapping dynamics upon protein binding. Therefore, we argue that more work is required to fully understand how protein binding influences DNA HT in the antennapedia homeodomain and *Pvu*II experiments.

Because the NCP is the fundamental building block of chromatin in the eukaryotic nucleus, the results of our experiments have several implications for the effects of DNA packaging on DNA HT in cellulo. For instance, the enhancement of damage in the most tightly packaged nucleosomes could result in enhanced guanine oxidation in heterochromatin versus euchromatin. Posttranslational modifications of the histone proteins, particularly those involving residues in the N-terminal tails, also regulate NCP stability and structure.[83] Therefore, experiments that explore the impact of histone tail acetylation on DNA HT in the NCP are of future interest. Also, the interactions between the histone tails and nucleosomal DNA are different in mononucleosomes and oligonucleosome arrays,[84] indicating that DNA HT experiments in dinucleosome and multinucleosome arrays are also of interest. A second important conclusion drawn from our experiments is that the distribution of guanine oxidation products is modulated by nucleosomal packaging. Therefore, the spectrum of guanine lesions generated by DNA oxidation could vary in different regions of chromatin. Recent experiments[85] have demonstrated that base excision repair of 8OG in NCPs is significantly impaired, so our observation that there may be an increased amount of this lesion in regions of tightly packaged chromatin has implications for the role of DNA hole transport in mutagenesis and carcinogenesis.

In conclusion, using a combination of well-established techniques to modulate nucleosome structure, we have demonstrated that DNA HT can be utilized to interrogate global changes in DNA−protein interactions. The fact that DNA HT dynamics in the AQ-601 construct are controlled by the rates of hole trapping, and not hole hopping, allows us to observe changes in the interaction of the histone N-terminal tails with nucleosomal DNA. This association leads to dramatic changes in long-range guanine oxidation yields and the spectrum of guanine oxidation products at low salt, but after tail dissociation at higher salt concentrations, the dynamics of DNA HT are very similar in naked and NCP constructs. Further, the modulation of DNA HT in both naked AQ-601 and rAQ-601 appears to be due to changes in the rate of reaction between the guanine radical cation and oxygen. These environmental effects on DNA HT have important implications for the control of guanine oxidation dynamics in cellulo, in solution, and in solid state device applications.

■ ASSOCIATED CONTENT

Ⓢ Supporting Information

A native PAGE gel showing the reconstitution efficiency of AQ-601 on native chicken erythrocyte nucleosome core particles (Figure S1), a native PAGE gel showing the reconstitution efficiency of AQ-601 on trypsinized chicken erythrocyte nucleosome core particles (Figure S2), a typical 7 M urea−6% PAGE DNA sequencing gel showing the salt dependence of DNA HT in naked AQ-601 and rAQ-601 samples as a function of salt concentration (Figure S3), and an autoradiograph of a representative 7 M urea−6% PAGE DNA sequencing gel showing the piperidine- and FPG-sensitive oxidation products observed following DNA HT in naked AQ-601, rAQ-601, and trAQ-601 at 10 mM NaCl (Figure S4). This material is available free of charge via the Internet at http://pubs.acs.org.

■ AUTHOR INFORMATION

Corresponding Author

*E-mail: wbdavis@wsu.edu. Telephone: (509) 335-4930. Fax: (509) 335-9688.

Present Address

[†]M. D. Anderson Cancer Center, Houston, TX 77030.

Funding

This material is based upon work supported by the National Science Foundation under CAREER Award 0347270 (W.B.D.).

Notes

The authors declare no competing financial interest.

■ ABBREVIATIONS

AQ, anthraquinone; EMSA, electrophoretic mobility shift assay; FPG, formamidopyrimidine DNA glycosylase; $G^{\bullet+}$, guanine radical cation; HT, hole transport; NCP, nucleosome core particle; rAQ-601, AQ-601-reconstituted nucleosome; SEM, standard error of the mean; trAQ-601, tailless AQ-601 nucleosome.

■ REFERENCES

(1) Genereux, J. C., Boal, A. K., and Barton, J. K. (2010) DNA-mediated charge transport in redox sensing and signaling. *J. Am. Chem. Soc. 132*, 891−905.

(2) Giese, B. (2002) Long-distance electron transfer through DNA. *Annu. Rev. Biochem. 71*, 51−70.

(3) Schuster, G. B., Ed. (2004) *Long-Range Charge Transfer in DNA*, Vols. *236−237*, Springer, Heidelberg, Germany.

(4) Wagenknecht, H.-A., Ed. (2005) *Charge Transfer in DNA*, Wiley-VCH, Weinheim, Germany.

(5) Berlin, Y. A., Burin, A. L., and Ratner, M. A. (2002) Elementary steps for charge transport in DNA: Thermal activation vs. tunneling. *Chem. Phys. 275*, 61−74.

(6) Bixon, M., and Jortner, J. (2006) Shallow traps for thermally induced hole hopping in DNA. *Chem. Phys. 326*, 252−258.

(7) O'Neill, M. A., and Barton, J. K. (2004) DNA Charge Transport: Conformationally Gated Hopping through Stacked Domains. *J. Am. Chem. Soc. 126*, 11471−11483.

(8) Voityuk, A. A. (2009) Can Charge Transfer in DNA Significantly Be Modulated by Varying the π Stack Conformation? *J. Phys. Chem. B 113*, 14365−14368.

(9) Kubar, T., and Elstner, M. (2008) What governs the charge transfer in DNA? The role of DNA conformation and environment. *J. Phys. Chem. B 112*, 8788−8798.

(10) Barnett, R. N., Cleveland, C. L., Joy, A., Landman, U., and Schuster, G. B. (2001) Charge Migration in DNA: Ion-Gated Transport. *Science 294*, 567−571.

(11) Seidel, C. A. M., Schulz, A., and Sauer, M. H. M. (1996) Nucleobase-specific quenching of fluorescent dyes. 1. Nucleobase one-electron redox potentials and their correlation with static and dynamic quenching efficiencies. *J. Phys. Chem. 100*, 5541−5553.

(12) Sistare, M. F., Codden, S. J., Heimlich, G., and Thorp, H. H. (2000) Effects of Base Stacking on Guanine Electron Transfer: Rate Constants for G and GG Sequences of Oligonucleotides from Catalytic Electrochemistry. *J. Am. Chem. Soc. 122*, 4742−4749.

(13) Lewis, F. D., Liu, J. Q., Zuo, X. B., Hayes, R. T., and Wasielewski, M. R. (2003) Dynamics and Energetics of Single-Step Hole Transport in DNA Hairpins. *J. Am. Chem. Soc. 125*, 4850−4861.

(14) Voityuk, A., Jortner, J., Bixon, M., and Rösch, N. (2000) Energetics of hole transfer in DNA. *Chem. Phys. Lett. 324*, 430−434.

(15) Liu, C. S., Hernandez, R., and Schuster, G. B. (2004) Mechanism for radical cation transport in duplex DNA oligonucleotides. *J. Am. Chem. Soc. 126*, 2877−2884.

(16) Osakada, Y., Kawai, K., Fujitsuka, M., and Majima, T. (2006) Charge transfer through DNA nanoscaled assembly programmable with DNA building blocks. *Proc. Natl. Acad. Sci. U.S.A. 103*, 18072−18076.

(17) Misiaszek, R., Crean, C., Joffe, A., Geacintov, N. E., and Shafirovich, V. (2004) Oxidative DNA damage associated with combination of guanine and superoxide radicals and repair mechanisms via radical trapping. *J. Biol. Chem. 279*, 32106−32115.

(18) Giese, B., and Spichty, M. (2000) Long Distance Charge Transport through DNA: Quantification and Extension of the Hopping Model. *ChemPhysChem 1*, 195−198.

(19) Nunez, M. E., Holmquist, G. P., and Barton, J. K. (2001) Evidence for DNA charge transport in the nucleus. *Biochemistry 40*, 12465−12471.

(20) Merino, E. J., and Barton, J. K. (2008) DNA oxidation by charge transport in mitochondria. *Biochemistry 47*, 1511−1517.

(21) Merino, E. J., Davis, M. L., and Barton, J. K. (2009) Common mitochondrial DNA mutations generated through DNA-mediated charge transport. *Biochemistry 48*, 660−666.

(22) Rajski, S. R., and Barton, J. K. (2001) How different DNA-binding protiens affect long-range oxidative damage to DNA. *Biochemistry 40*, 5556−5564.

(23) Lee, P. E., Demple, B., and Barton, J. K. (2009) DNA-mediated redox signaling for transcriptional activation of SoxR. *Proc. Natl. Acad. Sci. U.S.A. 106*, 13164−13168.

(24) Rajski, S. R., Kumar, S., Roberts, R. J., and Barton, J. K. (1999) Protein-mediated DNA electron transfer. *J. Am. Chem. Soc. 121*, 5615−5616.

(25) Nakatani, K., Dohno, C., Ogawa, A., and Saito, I. (2002) Suppression of DNA-mediated charge transport by BamHI binding. *Chem. Biol. 9*, 361−366.

(26) Boon, E. M., Pope, M. A., Williams, S. D., David, S. S., and Barton, J. K. (2002) DNA-mediated charge transport as a probe of MutY/DNA interaction. *Biochemistry 41*, 8464−8470.

(27) Nunez, M. E., Noyes, K. T., and Barton, J. K. (2002) Oxidative charge transport through DNA in nucleosome core particles. *Chem. Biol. 9*, 403−415.

(28) Bjorklund, C. C., and Davis, W. B. (2006) Attenuation of DNA charge transport by compaction into a nucleosome core particle. *Nucleic Acids Res. 34*, 1836−1846.

(29) Bjorklund, C. C., and Davis, W. B. (2007) Stable DNA-protein cross-links are products of DNA charge transport in a nucleosome core particle. *Biochemistry 46*, 10745−10755.

(30) Voityuk, A. A., and Davis, W. B. (2007) Hole Transfer Energetics in Structurally Distorted DNA: The Nucleosome Core Particle. *J. Phys. Chem. B 111*, 2976−2985.

(31) Andrews, A. J., and Luger, K. (2011) Nucleosome structure(s) and stability: Variations on a theme. *Annu. Rev. Biophys. 40*, 99−117.

(32) Grewal, S. I., and Moazed, D. (2003) Heterochromatin and epigenetic control of gene expression. *Science 301*, 798−802.

(33) Zheng, C., and Hayes, J. J. (2003) Structures and interactions of the core histone tail domains. *Biopolymers 68*, 539−546.

(34) Davis, W. B., Bjorklund, C. C., and Cho, P. S. (2010) Hole Transport Dynamics in Mixed Sequence DNA Can Vary with Salt Concentration: An Experimental and Theoretical Analysis. *J. Phys. Chem. C 114*, 20821−20833.

(35) Margolin, Y., and Dedon, P. C. (2010) A general method for quantifying sequence effects on nucleobase oxidation in DNA. *Methods Mol. Biol. 610*, 325−340.

(36) Gasper, S. M., and Schuster, G. B. (1997) Intramolecular photoinduced electron transfer to anthraquinones linked to duplex DNA: The effect of gaps and traps on long-range radical cation migration. *J. Am. Chem. Soc. 119*, 12762−12771.

(37) Lowary, P. T., and Widom, J. (1998) New DNA sequence rules for high affinity binding to histone octamer and sequence-directed nucleosome positioning. *J. Mol. Biol. 276*, 19−42.

(38) Hoch, D. A., Stratton, J. J., and Gloss, L. M. (2007) Protein-protein Forster resonance energy transfer analysis of nucleosome core particles containing H2A and H2A.Z. *J. Mol. Biol. 371*, 971−988.

(39) Mangenot, S., Leforestier, A., Vachette, P., Durand, D., and Livolant, F. (2002) Salt-induced conformation and interaction changes of nucleosome core particles. *Biophys. J. 82*, 345−356.

(40) Makde, R. D., England, J. R., Yennawar, H. P., and Tan, S. (2010) Structure of RCC1 chromatin factor bound to the nucleosome core particle. *Nature 467*, 562−566.

(41) Vasudevan, D., Chua, E. Y., and Davey, C. A. (2010) Crystal structures of nucleosome core particles containing the '601' strong positioning sequence. *J. Mol. Biol. 403*, 1−10.

(42) Humphrey, W., Dalke, A., and Schulten, K. (1996) VMD: Visual Molecular Dynamics. *J. Mol. Graphics 14*, 33−38.

(43) Lu, X.-J., and Olson, W. K. (2003) 3DNA: A software package for the analysis, rebuilding and visualization of three-dimensional nucleic acid structures. *Nucleic Acids Res. 31*, 5108−5121.

(44) Bohm, L., Briand, G., Sautiere, P., and Crane-Robinson, C. (1982) Proteolytic digestion studies of chromatin core-histone

structure. Identification of limit peptides from histone H2B. *Eur. J. Biochem. 123*, 299−303.
(45) Bohm, L., Briand, G., Sautiere, P., and Crane-Robinson, C. (1981) Proteolytic digestion studies of chromatin core-histone structure. Identification of a limit peptide of histone H3 and H4. *Eur. J. Biochem. 119*, 67−74.
(46) Bohm, L., Crane-Robinson, C., and Sautiere, P. (1980) Proteolytic digestion studies of chromatin core-histone structure. Identification of a limit peptide of histone H2A. *Eur. J. Biochem. 106*, 525−530.
(47) Bertin, A., Leforestier, A., Durand, D., and Livolant, F. (2004) Role of histone tails in the conformation and interactions of nucleosome core particles. *Biochemistry 43*, 4773−4780.
(48) Polach, K. J., Lowary, P. T., and Widom, J. (2000) Effects of core histone tail domains on the equilibrium constants for dynamic DNA site accessibility in nucleosomes. *J. Mol. Biol. 298*, 211−223.
(49) Cadet, J., Douki, T., and Ravanat, J.-L. (2008) Oxidatively Generated Damage to the Guanine Moiety of DNA: Mechanistic Aspects and Formation in Cells. *Acc. Chem. Res. 41*, 1075−1083.
(50) Reynisson, J., and Steenken, S. (2002) DFT calcultaions on the electrophillic reaction with water of the guanine and adenine radical cations. A model for the situation in DNA. *Phys. Chem. Chem. Phys. 4*, 527−532.
(51) Yun, B. H., Lee, Y. A., Kim, S. K., Kuzmin, V., Kolbanovskiy, A., Dedon, P. C., Geacintov, N. E., and Shafirovich, V. (2007) Photosensitized oxidative DNA damage: From hole injection to chemical product formation and strand cleavage. *J. Am. Chem. Soc. 129*, 9321−9332.
(52) Burrows, C. J., and Muller, J. G. (1998) Oxidative Nucleobase Modifications Leading to Strand Scission. *Chem. Rev. 98*, 1109−1152.
(53) Cullis, P. M., Malone, M. E., and Merson-Davies, L. A. (1996) Guanine Radical Cations Are Precursors of 7,8-Dihydro-8-oxo-2′-deoxyguanosine but Are Not Precursors of Immediate Strand Breaks in DNA. *J. Am. Chem. Soc. 118*, 2775−2781.
(54) Duarte, V., Gasparutto, D., Jaquinod, M., and Cadet, J. (2000) In vitro DNA synthesis opposite oxazolone and repair of this DNA damage using modified oligonucleotides. *Nucleic Acids Res. 28*, 1555−1563.
(55) Spassky, A., and Angelov, D. (1997) Influence of the local helical conformation on the guanine modifications generated from one-electron DNA oxidation. *Biochemistry 36*, 6571−6576.
(56) Spassky, A., and Angelov, D. (2002) Temperature-dependence of UV laser one-electron oxidative guanine modifications as a probe of local stacking fluctuations and conformational transitions. *J. Mol. Biol. 323*, 9−15.
(57) Kan, Y., and Schuster, G. B. (1999) Long-Range Guanine Damage in Single-Stranded DNA: Charge Transport through a Duplex Bridge and in a Single-Stranded Overhang. *J. Am. Chem. Soc. 121*, 10857−10864.
(58) Henderson, P. T., Jones, D., Hampikian, G., Kan, Y., and Schuster, G. B. (1999) Long-distance charge transport in duplex DNA: The phonon-assisted polaron-like hopping mechanism. *Proc. Natl. Acad. Sci. U.S.A. 96*, 8353−8358.
(59) Voityuk, A. A., Siriwong, K., and Rosch, N. (2004) Environmental fluctuations facilitate electron-hole transfer from guanine to adenine in DNA π stacks. *Angew. Chem., Int. Ed. 43*, 624−627.
(60) Hatcher, E., Balaeff, A., Keinan, S., Venkatramani, R., and Beratan, D. N. (2008) PNA versus DNA: effects of structural fluctuations on electronic structure and hole transport mechanisms. *J. Am. Chem. Soc. 130*, 11752−11761.
(61) Voityuk, A. A. (2008) Electronic couplings and on-site energies for hole transfer in DNA: Systematic quantum mechanical/molecular dynamic study. *J. Chem. Phys. 128*, 115101.
(62) Troisi, A., and Orlandi, G. (2001) The hole transfer in DNA: Calculation of electron coupling between close bases. *Chem. Phys. Lett. 344*, 509−518.
(63) Grozema, F. C., Tonzani, S., Berlin, Y. A., Schatz, G. C., Siebbeles, L. D., and Ratner, M. A. (2008) Effect of structural dynamics on charge transfer in DNA hairpins. *J. Am. Chem. Soc. 130*, 5157−5166.
(64) van Stroe, A. J., and Janssen, L. J. J. (1993) Determination of the diffusion coefficient of oxygen in sodium chloride solutions with a transient pulse technique. *Anal. Chim. Acta 279*, 213−219.
(65) Ju, L.-K., and Ho, C. S. (1985) Measuring oxygen diffusion coefficients with polarographic oxygen electrodes: I. Electrolyte solutions. *Biotechnol. Bioeng. 27*, 1495−1499.
(66) Li, G., Levitus, M., Bustamante, C., and Widom, J. (2005) Rapid spontaneous accessibility of nucleosomal DNA. *Nat. Struct. Mol. Biol. 12*, 46−53.
(67) Li, G., and Widom, J. (2004) Nucleosomes facilitate their own invasion. *Nat. Struct. Mol. Biol. 11*, 763−769.
(68) Koopmans, W. J., Buning, R., Schmidt, T., and van Noort, J. (2009) spFRET using alternating excitation and FCS reveals progressive DNA unwrapping in nucleosomes. *Biophys. J. 97*, 195−204.
(69) Wang, X., and Hayes, J. J. (2006) Physical methods used to study core histone tail structures and interactions in solution. *Biochem. Cell Biol. 84*, 578−588.
(70) Smith, R. M., and Rill, R. L. (1989) Mobile histone tails in nucleosomes. Assignments of mobile segments and investigations of their role in chromatin folding. *J. Biol. Chem. 264*, 10574−10581.
(71) Hill, C. S., and Thomas, J. O. (1990) Core histone-DNA interactions in sea urchin sperm chromatin. The N-terminal tail of H2B interacts with linker DNA. *Eur. J. Biochem. 187*, 145−153.
(72) Ballestar, E., Boix-Chornet, M., and Franco, L. (2001) Conformational changes in the nucleosome followed by the selective accessibility of histone glutamines in the transglutaminase reaction: Effects of ionic strength. *Biochemistry 40*, 1922−1929.
(73) Mutskov, V., Gerber, D., Angelov, D., Ausio, J., Workman, J., and Dimitrov, S. (1998) Persistent interactions of core histone tails with nucleosomal DNA following acetylation and transcription factor binding. *Mol. Cell. Biol. 18*, 6293−6304.
(74) Cary, P. D., Moss, T., and Bradbury, E. M. (1978) High-resolution proton-magnetic-resonance studies of chromatin core particles. *Eur. J. Biochem. 89*, 475−482.
(75) Ballestar, E., and Franco, L. (1997) Use of the transglutaminase reaction to study the dissociation of histone N-terminal tails from DNA in nucleosome core particles. *Biochemistry 36*, 5963−5969.
(76) Baneres, J. L., Martin, A., and Parello, J. (1997) The N tails of histones H3 and H4 adopt a highly structured conformation in the nucleosome. *J. Mol. Biol. 273*, 503−508.
(77) Lee, K. M., and Hayes, J. J. (1997) The N-terminal tail of histone H2A binds to two distinct sites within the nucleosome core. *Proc. Natl. Acad. Sci. U.S.A. 94*, 8959−8964.
(78) Yang, Z., Zheng, C., and Hayes, J. J. (2007) The core histone tail domains contribute to sequence-dependent nucleosome positioning. *J. Biol. Chem. 282*, 7930−7938.
(79) Hayes, J. J., Tullius, T. D., and Wolffe, A. P. (1990) The structure of DNA in a nucleosome. *Proc. Natl. Acad. Sci. U.S.A. 87*, 7405−7409.
(80) Svoboda, P., and Harms-Ringdahl, M. (2005) Influence of chromatin structure and radical scavengers on yields of radiation-induced 8-oxo-dG and DNA strand breaks in cellular model systems. *Radiat. Res. 164*, 303−311.
(81) Cloutier, J. F., Castonguay, A., O'Connor, T. R., and Drouin, R. (2001) Alkylating agent and chromatin structure determine sequence context-dependent formation of alkylpurines. *J. Mol. Biol. 306*, 169−188.
(82) Uberbacher, E. C., Ramakrishnan, V., Olins, D. E., and Bunick, G. J. (1983) Neutron scattering studies of nucleosome structure at low ionic strength. *Biochemistry 22*, 4916−4923.
(83) Eberharter, A., and Becker, P. B. (2002) Histone acetylation: A switch between repressive and permissive chromatin. Second in review series on chromatin dynamics. *EMBO Rep. 3*, 224−229.
(84) Zheng, C., and Hayes, J. J. (2003) Intra- and inter-nucleosomal protein-DNA interactions of the core histone tail domains in a model system. *J. Biol. Chem. 278*, 24217−24224.

(85) Menoni, H., Gasparutto, D., Hamiche, A., Cadet, J., Dimitrov, S., Bouvet, P., and Angelov, D. (2007) ATP-dependent chromatin remodeling is required for base excision repair in conventional but not in variant H2A.Bbd nucleosomes. *Mol. Cell. Biol. 27*, 5949−5956.